Ultrasonics 50 (2010) 666–674

Contents lists available at ScienceDirect

Ultrasonics

journal homepage: www.elsevier.com/locate/ultras

Ultrasonic transcutaneous energy transfer using a continuous wave 650 kHz Gaussian shaded transmitter

Shaul Ozeri [a], Doron Shmilovitz [a,*], Sigmond Singer [a], Chua-Chin Wang [b]

[a] School of Electrical Engineering, Tel-Aviv University, Israel
[b] Dept. of Electrical Engineering, National Sun Yat-Sen University, Taiwan

ARTICLE INFO

Article history:
Received 9 December 2009
Received in revised form 13 January 2010
Accepted 13 January 2010
Available online 6 February 2010

Keyword:
Ultrasonic transcutaneous energy transfer

ABSTRACT

This paper proposes ultrasonic transcutaneous energy transfer (UTET) based on a kerfless transmitter with Gaussian radial distribution of its radiating surface velocity. UTET presents an attractive alternative to electromagnetic TET, where a low power transfer density of less than 94 mW/cm^2 is sufficient. The UTET is operated with a continuous wave at 650 kHz and is intended to power devices implanted up to 50 mm deep. The transmitter was fabricated using a 15 mm diameter disc shape PZT (Lead Zirconate Titanate) element (C-2 grade, Fujiceramics Corporation Tokyo Japan), in which one surface electrode was partitioned into six equal area electrodes (~23 mm^2 each) in the shape of six concentric elements. The UTET was experimented using pig muscle tissue, and showed a peak power transfer efficiency of 39.1% at a power level of 100 mW. An efficient (91.8%) power driver for the excitation of the transmitter array, and an efficient rectifier (89%) for the implanted transducer are suggested.

To obtain the pressure field shape, the Rayleigh integral has been solved numerically and the results were compared to finite element simulation results. Pressure and power transfer measurements within a test tank further confirm the effectiveness of the proposed UTET.

1. Introduction

Transcutaneous energy transfer (TET) is a technique used to remotely power implanted devices. Presently existing TET devices implement electromagnetic power coupling between external and implanted coils featuring power transfer of up to 10 W [1–4]. For transferring power with power density of up to 94 mW/cm^2, an ultrasonic transcutaneous energy transfer (UTET) based on transmitting ultrasonic waves can be used [5,6]. Using ultrasonic waves rather than electromagnetic waves has the benefit of being less susceptible to nearby ferromagnetic materials, in addition to exhibiting high power transfer efficiency (27%) [6]. A straightforward realization of a UTET is presented by [6], using a flat circular piezoelectric ultrasonic transmitter feeding an implanted piezoelectric receiver by the acoustic waves of 673 kHz. In such a realization of UTET, the transmitting element is electrically excited to impose a uniform electrical excitation, which in turn generates a uniform surface vibration velocity amplitude and phase over the radiating surface. The uniform transmitter's surface vibration has the advantage of having self natural focusing zone [8], and being simple to realize. However, beyond the self focusing zone, the intensity rapidly decreases at a rate proportional to $1/R^2$ (R stands for the distance from the radiating surface). That implies that a finite aperture size receiver (of approximately three wavelengths) can capture only part of the power transmitted. Furthermore, the beam profile contains alternate polarity side lobes [19] that reduce the available power at the receiver's terminals. To overcome the spreading of the wave's profile, ultrasonic devices such as imaging devices implement an apodization of the excitation waveform that forces a non-uniform radial distribution of the transmitter's radiating surface. Durnin and Miceli [10] showed (for an optical signal) that excitation in the shape of zero order Bessel function of the 1st kind, J_0 of an infinite aperture transducer, results in an Axicon which is a non-diffracting propagating wave. A practical implementation of the Bessel beam consists of a transducer having a finite aperture size that proves also to be effective [9,11]. Unfortunately, for continuous power transfer through a living tissue, the Bessel beam has two disadvantages. It generates a pressure field that consists of a main lobe concentrated along the acoustic axis, and several (<10 depends on the accuracy of the Bessel stepwise approximation) lower amplitude (−0.4, +0.3, −0.25, +···, normalized to the amplitude of the main lobe) side lobes [7] that travel in parallel with the main lobe [9,19]. Side lobes tend to decrease the amount of energy harvested by the receiver as it has an alternating pressure polarity. The main lobe having a narrow width (that depends on the aperture to wavelength ratio), concentrates the wave's energy within the narrow tissue's cross section, and consequently might increase the intensity of the wave beyond the safety limit of 94 mW/cm^2 [12,13].

* Corresponding author.
E-mail address: shmilo@eng.tau.ac.il (D. Shmilovitz).

0041-624X/$ - see front matter © 2010 Elsevier B.V. All rights reserved.
doi:10.1016/j.ultras.2010.01.004

A preferred shading profile is the truncated Gaussian, that generates a diffraction field which is described by a Gaussian function [14,17]. Gaussian shading is based on an excitation voltage that decreases radially from the transducer's center with a Gaussian envelope truncated at the edges of the transducer. Gaussian shading generates an ultrasonic pressure field that, for UTET implementation, exhibits some advantages over a Bessel or uniform excitation. A Gaussian beam has reduced pressure variations in the near field compared to uniform excitation, side lobes suppression of better than 30 dB at the far field [14], and is reported to have an indistinguishable near field from far field [14]. These advantages make the Gaussian beam attractive for UTET devices, since the pressure field keeps its Gaussian shape for a long enough axial length (~50 mm in this work), while the energy carried by the ultrasonic waves can be spread over the entire cross section area of the medium, consequently reducing the wave's intensity (which is the power flow density) to a safe limit. Since the proposed UTET is intended for operation in a distance of up to 50 mm, the limited depth of field of the Gaussian compared to Bessel shaded transducer is tolerable.

Radial surface velocity distribution may be attained through several approaches, such as uniform excitation of a transducer with a radial distribution of the level of piezoelectric polarization [16,17], or use of a non-uniform radial excitation of a transducer composed of an array of concentric rings surrounding an inner concentric disc [18]. The second approach was chosen since it does not involve a complex piezoelectric material polarization procedure. Each element of the array is excited by its own voltage source with an amplitude level that corresponds to the desired step wise approximated Gaussian voltage mask. The pressure field generated by each element is calculated and all contributions are summed to build the overall pressure field.

The objective of this paper is to present a UTET which is capable of transferring power efficiently to a distance of up to 50 mm by using a kerfless annular implementation of the transmitter. This work presents a detailed design analysis of a continuous wave (CW) constant frequency 650 kHz Gaussian shaded UTET device. The paper starts with a numerical solution of the Rayleigh double integral which was compared to a finite element simulation using Comsol Multiphysics (Comsol Multiphysics, Comsol AB, Stockholm Sweden). The paper then presents the fabrication of a six elements annular transmitter, the design of an efficient power driver array (91.8%) and an efficient receiver's rectifier (89%). Finally measurement results of power transfer of a 100 mW through pig muscle tissue are presented. Measurements were done for an axial distance of up to 50 mm, while measuring its sensitivity to lateral shift between the transducers.

2. Numerical calculation of the pressure field

The UTET link was constructed using flat circular transducers for the implementation of the transmitters that have a spatially varying particle velocity on the radiating surface, producing a beam pattern that is very different from transmitters with a uniform velocity distribution. The formal expression describing the pressure field of such transmitters is given by the Rayleigh surface integral [7,8,15] which accounts for diffraction from an arbitrary source. The approach is based on the summation of spherical wave contributions from each point source on the radiating surface.

$$P(x,y,z;t) = \frac{jk\rho_0 c_0}{\pi}\int_S v(x',y')\frac{e^{-jkR}}{R}dS \quad (1)$$

$$R = \sqrt{(x-x')^2+(y-y')^2+z^2} \quad (2)$$

$$k = \frac{2\pi}{\lambda} \quad (3)$$

where $v(x', y', z = 0)$ is the vibration velocity normal to the transducer's radiating surface, $L(x,y,z)$ is an observation point in front of the transducer, k is the wave number, λ is the wavelength of the pressure wave in the tissue (~2.3 mm at 650 kHz), c_0 is the average speed of sound (wave's phase velocity) in the medium in front of the transducer, ρ_0 is the average density of the medium, and S is the transducer area. R is the distance from a point source $(x', y', 0)$ on the transducer's radiating surface to the observation point $L(x,y,z)$. This technique is applicable also to the UTET since the UTET device operates at a low peak excitation electrical field of ~6.6 V/mm where the behavior of the transducer remains linear [30].

Obtaining an exact general analytical solution to (1) that would cover the whole space in front of the radiating surface S is almost impossible, therefore solutions are based on simplifying assumptions such as solving (1) for observation points that are far enough from the transducer [7,8]. Further approximation is done by assuming a transducer aperture which is much greater than the ultrasonic wavelength [8,15].

2.1. Pressure field generated by a single plane ring

For a transmitter composed of an array of concentric elements, each element has a uniform surface vibration, so (1) can be simplified. The pressure field produced by a ring-shaped transducer at an observation point $L(x,y,z)$ in cylindrical coordinates is given by [7,8]:

$$P_{Ring}(x,y,z;t) = \frac{jk\rho_0 c_0 u_0}{2\pi}e^{j\omega t}\int_s \frac{e^{-jkR}}{R}ds \quad (4)$$

Using (2) and analytical geometry, R can be described by:

$$R = \sqrt{r^2+a^2-2ra\sin\theta\cos\psi} \quad (5)$$

where 'r' is the distance from the center of the ring to the observation point L, 'a' is the average radius, $-0.5\pi < \theta < 0.5\pi$ is the angle of elevation from the acoustic axis and ψ is the integration angle through the ring's perimeter $0 \leqslant \psi < 2\pi$. dS is the area of a small vibrating source over the radiating surface (Fig. 1)with an area of $dS = wad\psi$

Actually, $\rho_0 c_0 = Z_0$ is the characteristic impedance of the medium and $\rho_0 c_0 u_0 = P_0$ has the meaning of pressure in Pa. Also, the integral given by (4) is reduced to a one dimensional integral and, taking advantage of the cylindrical symmetry, the limits of integration can be reduced to ($\psi \in [0, \pi]$):

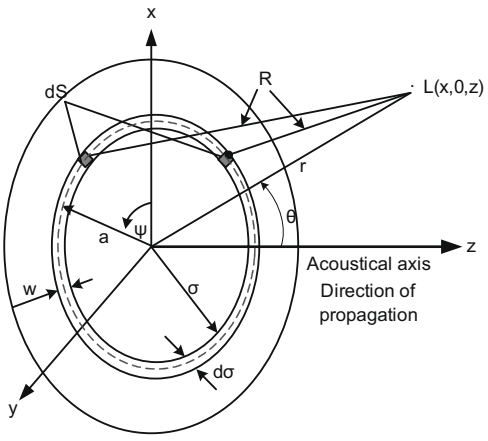

Fig. 1. Calculation of the pressure field generated by a ring and disc transducer.

$$P_{Ring} = \frac{2jkawP_0e^{j\omega t}}{\pi}\int_0^{\pi}\frac{e^{-jkR}}{R}d\psi = \frac{2jkawP_0e^{j\omega t}}{\pi}\int_0^{\pi}\frac{e^{-jk\sqrt{r^2+a^2-2ra\sin\theta\cos\psi}}}{\sqrt{r^2+a^2-2ra\sin\theta\cos\psi}}d\psi \quad (6)$$

By defining:

$$A = \frac{2ra\sin\theta}{r^2+a^2} \quad (7)$$

The pressure expression becomes:

$$P_{Ring} = \frac{2jkawP_0e^{j\omega t}}{\pi\sqrt{r^2+a^2}}\int_0^{\pi}\frac{e^{-jk\sqrt{r^2+a^2}\sqrt{1-A\cos\psi}}}{\sqrt{1-A\cos\psi}}d\psi \quad (8)$$

A similar approach gives the pressure generated by a disc shape transducer:

$$P_{Disc}(r,\theta,t) = \frac{jkP_0}{\pi}e^{j\omega t}\int_0^{\pi}d\psi\int_0^{a}\sigma\frac{e^{-jkR}}{R}d\sigma \quad (9)$$

A practical aperture size such as used in UTET is $a = 7.5$ mm and the wave number is $k \sim 2200$ 1/m. The pressure expression in (4) is very oscillatory and therefore cannot have a closed analytical solution. In addition, the technique known as stationary phase for the solution of integrals in the form of $I = \int_0^{\pi} f(\psi)e^{jb\phi(\psi)}d\psi$ is applicable only for the case of $b \to \infty$, but for the UTET $b = k\sqrt{r^2+a^2} = ka\sqrt{1+r^2/a^2}$ which leads to $10 \leqslant b \leqslant 50$. Since b is not sufficiently large, the stationary phase technique is also not applicable. Therefore, to evaluate the pressure field without gross assumptions, a numerical solution is adopted.

2.2. Determining the pressure field due to contributions of all of the array's elements

Since the electrode area is partitioned into six concentric elements with a narrow (~0.2 mm) clearance between adjacent elements, apodization is achieved by connecting each element's electrode to a separate excitation source. The excitation sources are designed to impose an excitation voltage according to a Gaussian mask. In practice, this is a gross stepwise approximation to the Gaussian profile since the surface area of the transducer is divided into a small number (six in this work) of concentric elements. A lesser number of elements might lead to a ring width having width–thickness ratio ~1, which might cause undesired lateral vibrations [22]. The Gaussian excitation amplitude $v(\bar{r})$ profile centered at the center of the transducer is in the form of:

$$v(\bar{r}) = e^{-\alpha\left(\frac{\bar{r}}{a}\right)^2} \quad (10)$$

where a is the transducer's aperture, α is the Gaussian constant, and $\bar{r}$ is the average concentric element's radius.

Since the surface velocity is proportional to the excitation voltage level, P_0 is also proportional to $v(\bar{r})$ and the expression of the pressure field P_L at observation point $L(x,y,z)$ due to the contribution of all rings is:

$$P_{Ring}(L,t) = \frac{2jk}{\pi}\times\sum_{n=1}^{N}\left(a_nw_nP_{0_n}\int_0^{\pi}\frac{e^{-jk\sqrt{r^2+a_n^2-2ra_n\sin\vartheta\cos\psi}}}{\sqrt{r^2+a_n^2-2ra_n\sin\vartheta\cos\psi}}d\psi\right)e^{j\omega t} \quad (11)$$

This expression was solved numerically by replacing the integration with a summation and its result has been added to the numerical solution of (9) which is the expression representing the contribution of the inner disc. $N = 5$ represents the number of concentric rings and n is the ring's index of summation $n \in [1, N]$

$$a : a_1, \ldots, a_N \quad (12)$$

$$f_{m,n}(r,\vartheta,\psi_m,a_n) = \frac{e^{-jk\sqrt{r^2+a_n^2-2ra_n\sin\vartheta\cos\psi_m}}}{\sqrt{r^2+a_n^2-2ra_n\sin\vartheta\cos\psi_m}} \quad (13)$$

$$P_L(r,\vartheta) = \frac{2jk}{\pi}\sum_{n=1}^{N}a_nw_nP_{0_n}\left(\sum_{m=1}^{M}f_{m,n}(r,\vartheta,\psi_m,a_n)\Delta\psi\right) \quad (14)$$

$$\Delta\psi = \frac{\pi}{M} \quad (15)$$

$$\psi_m = m\Delta\psi, \quad \psi : \psi_1, \ldots, \psi_M \quad (16)$$

$$\theta \in [-0.5\pi, 0.5\pi] \quad (17)$$

3. Experimental set-up and results

The UTET link was constructed using flat circular transducers for the implementation of the transmitter and the receiver. The excitation voltage was chosen to be a continuous wave with a frequency of 650 kHz, which is a frequency high enough to result in a receivers' thickness of less than 5 mm (including matching layer), and low enough to have a reasonable average soft tissue attenua-

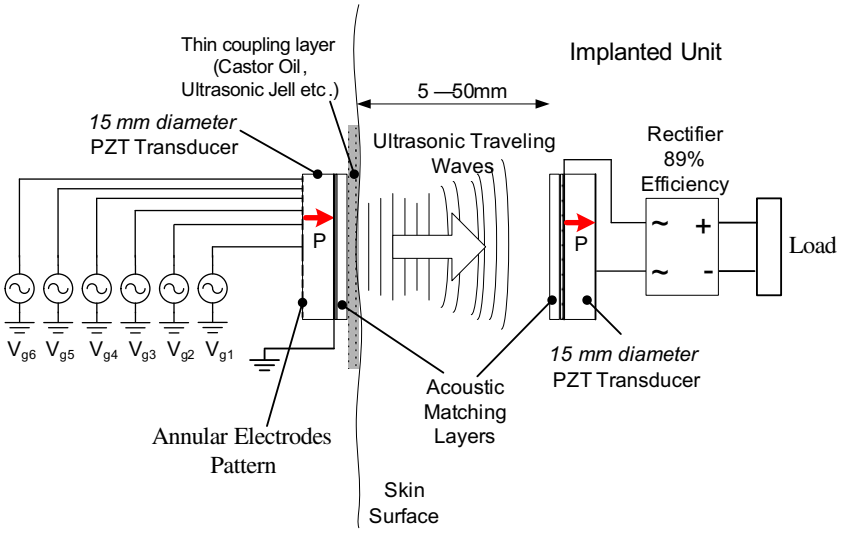

Fig. 2. Illustration of the proposed Gaussian shaded UTET.

Table 1
Transmitter's electrodes dimensions.

	Inner radius (mm)	Outer radius (mm)	Area (mm^2)	Width (mm)
Disc	0	2.7	22.90	2.7
Ring 1	2.9	3.96	22.84	1.06
Ring 2	4.16	4.96	22.93	0.8
Ring 3	5.16	5.82	22.78	0.66
Ring 4	6.02	6.6	22.93	0.58
Ring 5	6.8	7.32	23.06	0.52
Total area			137.44	

tion of about 0.5 dB/cm [28]. The ultrasonic field is designed to be confined inside a virtual cylindrical envelope lying between the transducers. In this way, the ultrasonic energy is spread over the entire cross section of the virtual cylinder, lowering the wave's peak intensity and helping to meet safety regulatory requirements [12,13]. Fig. 2 illustrates the architecture of the Gaussian shaded UTET.

Both transmitter and receiver have the same aperture size of 7.5 mm $\sim 3.3\lambda$ (λ is the wavelength of the pressure wave in the soft tissue medium), excited by a peak voltage of 20 V (Table 2 lists the actual excitation voltages that were needed to generate intensity of 94 mW/cm^2). In addition, the power transfer of the ultrasonic link was characterized using pig muscle tissue, at three (5 mm, 10 mm, 40 mm) thicknesses immersed in a test bath filled with distilled water, and the power transferred sensitivity to lateral shift (0–14 mm) at those distances was measured.

3.1. Transmitter fabrication

Fabrication of the transducer was based on a commercially available disc-shaped PZT (Lead Zirconate Titanate) elements purchased with both surfaces completely coated with thin silver layers (Z3T 15D-C2 piezoelectric properties close to PZT-4, manufactured by Fuji Ceramics Corporation, Tokyo Japan). Fig. 3 is an illustration of a single ring transmitter. To enable the use of a common return path for the switch-mode resonance power amplifier, the front electrode was left untouched as a common electrical return path and the back surface electrode was partitioned into five concentric rings, surrounding an inner disc. This is a kerfless implementation of the Gaussian excitation's quantization by six equal area ($\sim$22.9 mm^2) concentric elements which proved to be sufficient.

Table 2
Transmitter's excitation voltages (amplitudes). V_1 corresponds to the inner-most electrode.

	Peak excitation voltage [V]	Element
V_1	20	Disc
V_2	14.4	Ring 1
V_3	10.8	Ring 2
V_4	7.2	Ring 3
V_5	4	Ring 4
V_6	1.6	Ring 5

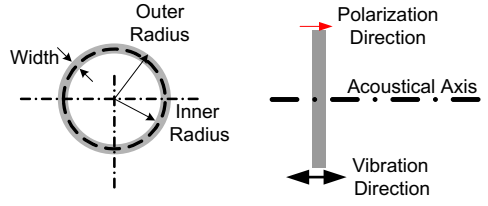

Fig. 3. Illustration of a ring transmitter.

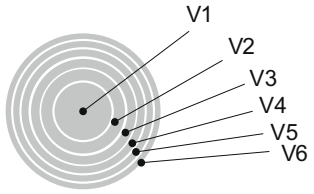

Fig. 4. Illustration of the electrode pattern with decreasing ring width to keep a constant ring area.

The radiated power strength depends on the radiating surface area, consequently implementation of equal area elements was chosen (Fig. 4) and the Gaussian shading was imposed on the excitation voltage. Table 1 presents the dimensions of the electrodes.

Since the electrodes were made of a silver layer which is difficult for laser beam etching due to the fast heat evacuation by the silver, a micromachining process (using a lathe) was used to remove thin 0.2 mm clearances between the electrodes by scratching the silver surface to a depth of 0.2 mm, and then electrical measurements were used to verify electrical discontinuity between adjacent electrodes.

3.2. Optimizing the acoustic coupling

The PZT material used as the electromechanical element has much higher acoustic impedance ($Z \sim 30$ MRayls, depending on the type of material) than soft tissue ($Z \sim 1.5$ MRayls). To improve the coupling of energy into the tissue, acoustic matching layers were added to the radiating surface of the PZT elements. The back surface was left open (air backed, $Z \sim 400$ Rayls), so only negligible ultrasonic energy escaped to the air from the back surface. The matching layers were fabricated as disc plates and glued using Hernon's Quantum 149 glue (manufactured by Hernon, Sanford Florida USA). A multiple matching layer technique has been implemented for the acoustic matching of both transmitter and receiver using Piezocad (Sonic Concepts Inc., Bothell WA USA). Fig. 5 illustrates the resulted construction of both transducers.

3.3. Receiver fabrication

The receiver was composed of the same circular PZT element as used for the transmitter (Fujiceramics Z3T 15D), with its silver electrode covering the front and back surfaces. A single layer quarter wavelength matching technique [20] was adopted as illustrated in Fig. 5. A 1.3 mm thick graphite disc (EK2200 made by SGL Carbon Group, Wiesbaden Germany) with a density of 1.82 g/cm^3 and a Young's modulus of 23 GPa. To compensate for the inaccuracy of the actual glue layer's thickness (designed to be 20 μm), the graphite layer thickness was calibrated after the cure of the glue (24 h). Although this type of carbon is not biocompatible, some types such as pyrolytic carbons can be used which are both biocompatible and hemocompatible [24–26]. PZT material is also not biocompatible (contains lead), but since the transducers are sealed, the tissue is exposed only to the outer surface of the matching layer. The receiver's electrical terminals were connected to a high efficiency rectifier ($\sim$89%) that extracted most of the harvested power.

3.4. Voltage mask

Each surface electrode was connected to a synchronized power amplifier having the same frequency and phase but generating different voltage amplitudes according to the Gaussian profile, as presented in Table 2 and Fig. 6:

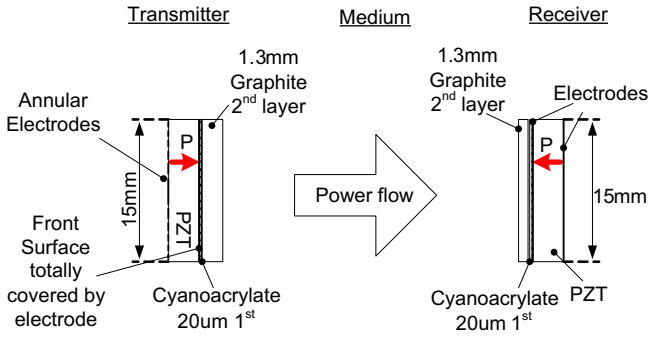

Fig. 5. Construction of transmitter and receiver. Actual medium used: soft tissue (pig muscle).

In contrast to a Bessel beam profile, all voltages share the same relative polarity.

3.5. Power amplifier array

There are two main requirements from the amplifier: to have greater than 90% power processing efficiency, and to be capable of voltage boost up to 20 Vpk (in this implementation). A switch-mode parallel resonance converter PRC topology is illustrated in Fig. 7 meeting those requirements.

The amplifier array was composed of six identical channels as illustrated in Fig. 7. To synchronize the channels, it was connected to the same common Fclk of complementary outputs x_1 and x_2 (45% duty cycle, 650 kHz). In the PRC the load is connected across the resonating capacitor. PRC has a voltage gain that depends on the operating frequency as shown in Fig. 8, and has a gain peak at the resonance frequency known as the quality factor Q given by:

$$Q = \frac{R_{load}}{\omega_0 L_r} = \frac{R_{load}}{\sqrt{L_r/C_r}} \tag{18}$$

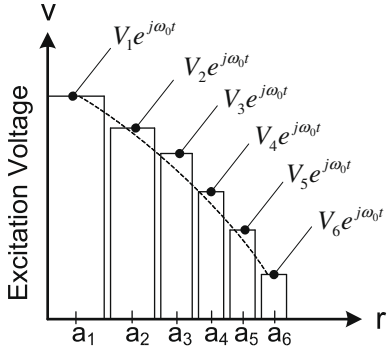

Fig. 6. Stepwise approximation of the Gaussian shading by the excitation voltage.

ω_0 is the angular resonance frequency given by:

$$\omega_0 = \frac{1}{\sqrt{L_r C_r}} \tag{19}$$

C_r is composed of the amplifier's network resonating capacitor (COG dielectric, multilayer, KEMET SC USA) in parallel with the capacitance imposed by the piezoelectric element.

The voltage gain is given by [31]:

$$G(j\omega) = \frac{V_{out}}{V_{in}}(j\omega) = \frac{1}{1 - \omega^2 L_r C_r + j\omega L_r / R_{load}} \tag{20}$$

The resonating LC network is being driven by a square wave (actually a trapezoidal wave approximated to a square wave since the rise and fall times are short enough (~30 ns), compared to the period of ~1.54 μs. The voltage driving the LC tank can be represented by a 50% duty cycle square wave Fourier series [31]:

$$V_{in}(t) = A\left(dc + \sin(2\pi ft) + \frac{1}{3}\sin(6\pi ft) + \frac{1}{5}\sin(10\pi ft) + \cdots\right) \tag{21}$$

A is a constant that depends on the square wave's peak amplitude. The dc component is blocked by the series blocking capacitor C_b, as shown in Fig. 7. The shape of the frequency response acts as a low pass filter by amplifying the fundamental signal (×6.75) and at the same time attenuating the harmonics, as illustrated in Fig. 9.

The actual attenuation is about −41.5 dB achieved within half an octave distance from the fundamental frequency. Fig. 10 shows the measured voltage and current waveforms of the PRC converter.

The PRC achieved a conversion efficiency of 91.8%. The efficiency was calculated by dividing the output power of the converter (power consumed by the piezoelectric element) by the power of the DC voltage source. The total harmonic distortion cal-

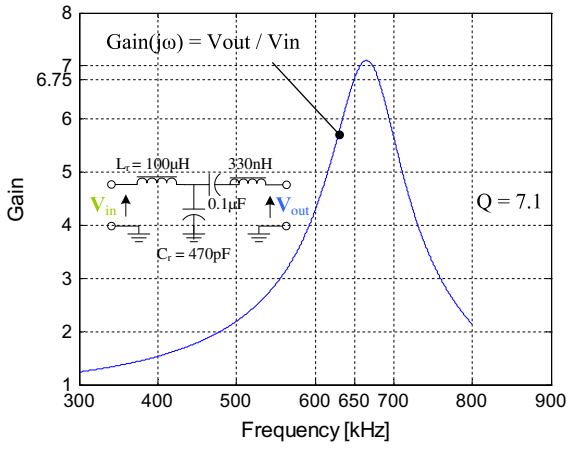

Fig. 8. Frequency response of the parallel resonance converter.

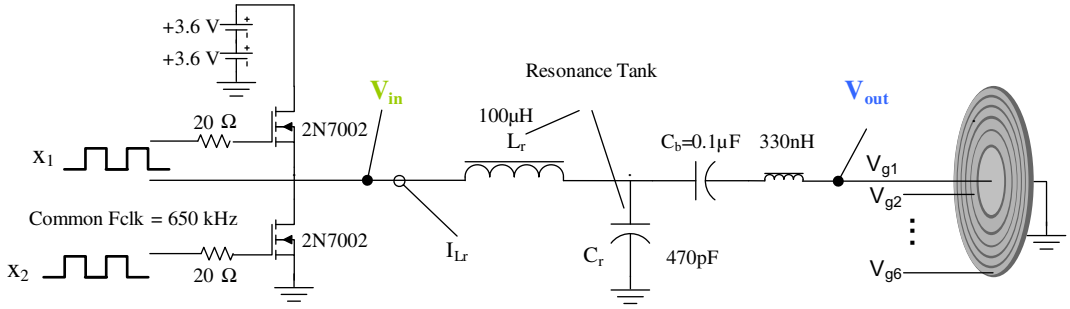

Fig. 7. One of six channels of the high efficiency (91.8%) power amplifier.

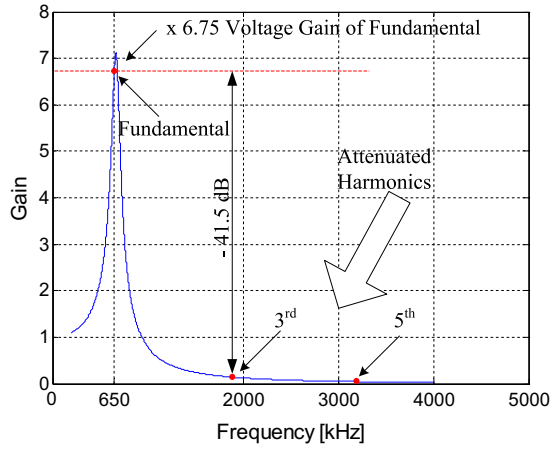

Fig. 9. 200 kHz–4 MHz frequency response of the PRC showing −41 dB attenuation of harmonics.

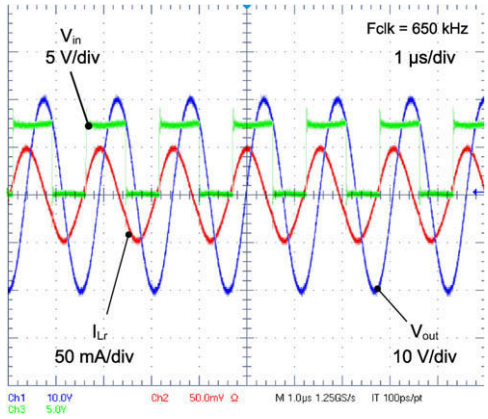

Fig. 10. Measured electrical waveforms of the 1st channel of the PRC converter array.

culated using the first fifty harmonics is 0.63%, which means that no spurious vibration mode of the transmitter is unintentionally excited.

3.6. High efficiency (89%) receiver's rectifier

Most implanted electrical loads that use a receiver's energy as an electrical source require DC voltage in the range of 1.2 V–3.3 V for its operation, such as an implantable micro stimulator [3]. Sometimes the receiver output energy is used to charge an implanted battery [4]. If a traditional two way diode rectifier and a smoothing capacitor are used to rectify the AC voltage generated by the receiver, poor energy extraction will result due to the non-linear behavior of the rectifier and the two diode's forward voltage drop [21]. The passive rectifier illustrated in Fig. 11 was built and the rectifier's output was loaded by an adjustable resistive load of 22 turns (3059 series, Bourns Riverside California) and tuned to give a +3.6 VDC (at ~180 Ω which is close to the matched transducer's series resistance). This voltage is high enough to enable the use of low dropout +3.3 V regulator which is a common logic circuitry supply voltage.

3.7. Finite element and Matlab simulation of the pressure field

To present a clear picture of the pressure field and the advantage of Gaussian shading over a flat uniform excitation, simulations

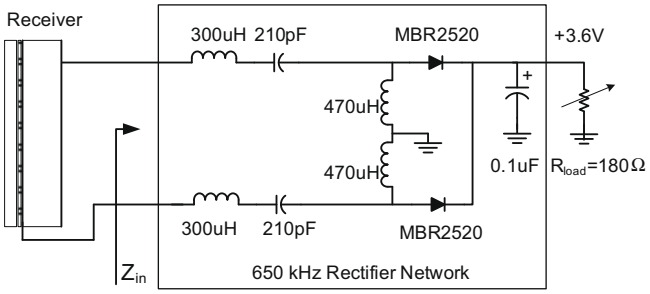

Fig. 11. High efficiency (89%) receiver's rectifier.

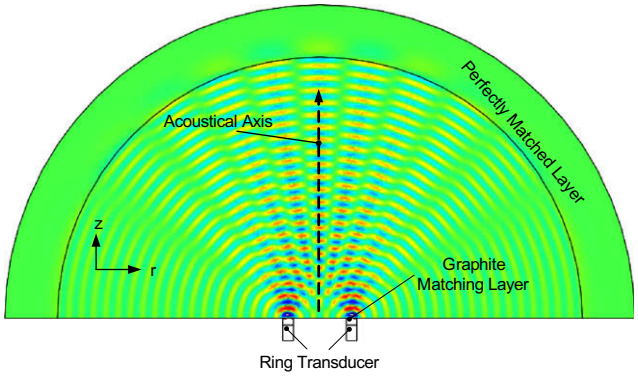

Fig. 12. 2D surface plot finite element simulation (Comsol Multiphysics) of the pressure map generated by a single ring.

were carried out using the finite element Comsol Multiphysics package to compare with the numerical solution of the expression given in (14). Simulations were done for a maximum propagating distance of 50 mm surrounded by a thin perfectly matched layer to avoid reflections. Since the Gaussian shading is implemented by radial partitioning of the transmitter's electrode, the simulation process started with the pressure field generated by a single ring radiator and the result is presented in Fig. 12. Vibration modes and characterization of a ring shape transducer are given in [22,27].

The simulation model included the piezoelectric element and its acoustic matching layers. To emphasize the advantage of a Gaussian shaded transducer over a uniformly excited disc radiator, the simulation result of a uniformly excited piston radiator is illustrated in Fig. 13 clearly illustrating the side lobes generated.

The pressure map of the Gaussian shaded transmitter 2D simulation illustrated in Fig. 14a and c are the result of the numerically solved expression given by (14), which clearly shows a pressure

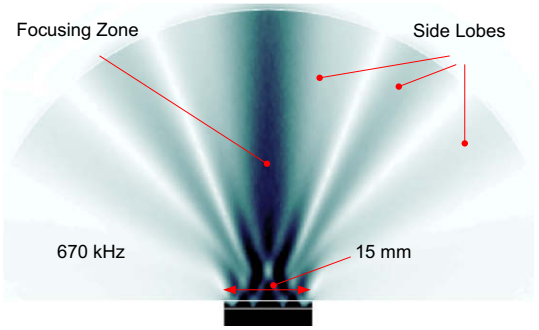

Fig. 13. 2D surface plot finite element simulation (Comsol Multiphysics) of the field's intensity map generated by a uniformly excited piston transducer.

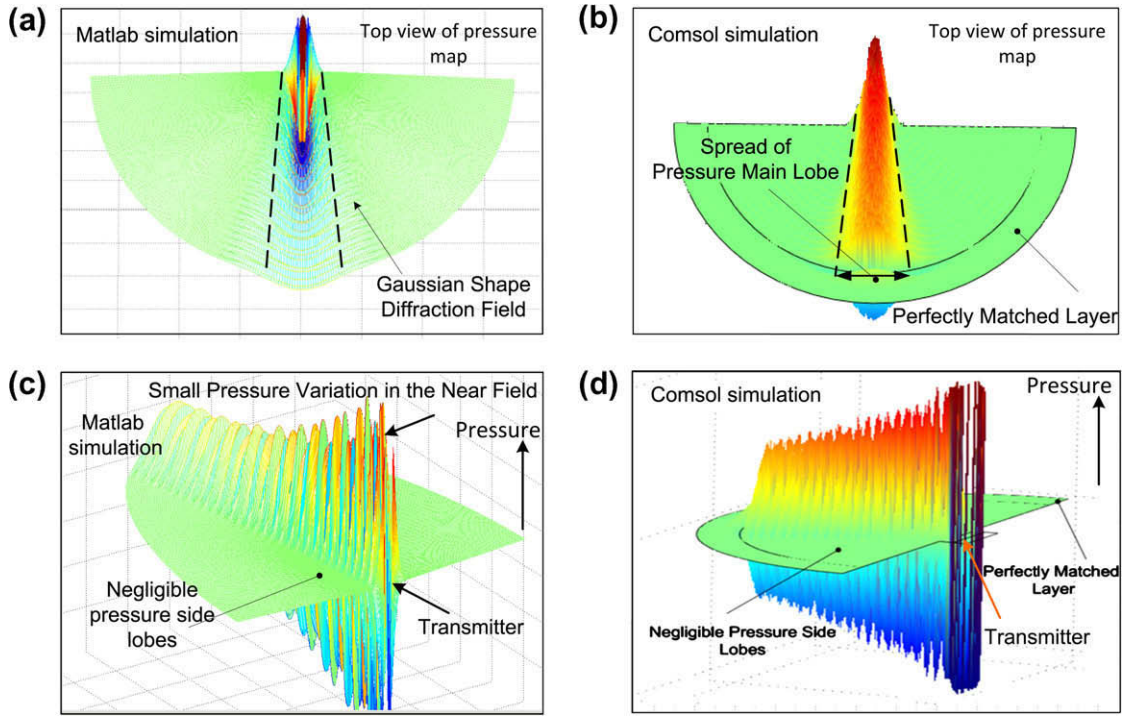

Fig. 14. (a) Matlab numerical solution, and (b) finite element simulation of the pressure field generated by the stepwise approximated Gaussian shaded transducer.

map that is similar to what is achieved by the finite element simulation given in (b and d).

Power transfer efficiency depends on the field intensity shape which is proportional to the pressure squared, therefore intensity is more concentrated than the pressure field. Maximum source power to DC load power efficiency achieved is 39.1% when the transmitter and receiver are optimally oriented (zero lateral shift between the transducers). Efficiency decreased to 17.2% at a distance of 40 mm as the result of accumulated tissue absorption and the spread of the field's intensity with the increased distance between the transducers. Power transfer efficiency was calculated by dividing the measured DC load power Pout by the transmitter's consumed power Pin. The transmitter's power was measured by using the multiplication feature of the oscilloscope to multiply the instantaneous transmitter's voltage and current of each concentric element, and then averaging the result. Electrical waveforms were recorded using a TDS5054, 500 MHz, four channel oscilloscope along with P5050 voltage probes and CT-2 current probes with a transducer sensitivity of 1 mV/mA (all of which are manufactured by Tektronix, Oregon, USA). The efficiency calculation included the rectifier loss that achieved a high efficiency of 89%, high enough not to need synchronous rectification.

To verify the performance of the UTET link, measurements of ultrasound radiation and energy transfer were conducted within a water tank, using water at a room temperature of 25 °C. Distilled water served as a medium for acoustic wave pressure measurements, since its acoustic impedance is close to that of soft biological tissue and allows the hydrophone to be easily moved in order to map the pressure pattern. This serves as a first-order proof-of-concept. The test tank was fabricated out of 6 mm thick Perspex plates and has dimensions of 40 × 20 × 20 cm. In order to avoid reflections from the test tank walls, these were covered with a 10 mm thick ultrasonic absorber sheet, Aptflex F28, attached to the internal side walls by APTBOND B1 bond (both manufactured by Precision Acoustics, Dorchester UK). Pressure was measured along the acoustic axis using a miniature hydrophone probe (TC4038, manufactured by Reson, Slangerup Denmark) which has a sensitivity of −224.5 dB ± 2 dB at 650 kHz re 1 V/μPa (−228 dB ± 2 dB at 100 kHz). Measurement results of the pressure amplitude recorded at intervals of 1 mm along the acoustic axis, generated by the Gaussian shaded transmitter, are presented in Fig. 15.

Although skin and the underlying soft tissue layer have acoustic impedances and phase velocities that are close to those of distilled water, the attenuation of the pressure field by tissue is much larger than water attenuation (soft tissue 0.6–1.5 dB/cm compared to water 0.002 dB/cm at 1 MHz) [28,29]. To account for the tissue losses, power transfer measurements were conducted using bulk pig muscle tissue (abdominal) [23] that was immersed in the water inside the test tank between the transmitter and receiver. Fig. 16 shows the measured output power and calculated efficiency as a function of the tissue (pig muscle, ~1.8 dB/cm at 1 MHz) thickness *d*, and lateral shift *Ls*. Transmitter power of Pin = 256 mW was kept constant as a power reference during all load power measurements, since it yielded a load power of 100 mW at the shortest distance *d* of 5 mm.

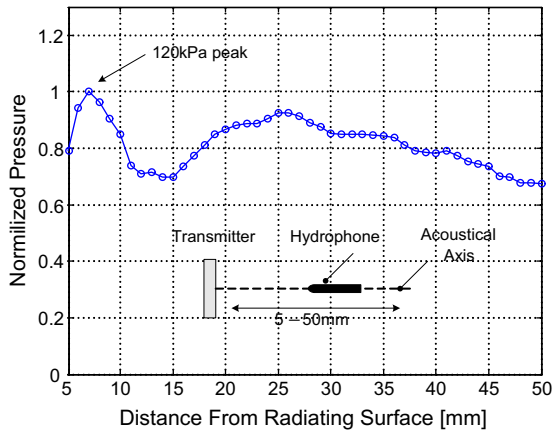

Fig. 15. Pressure measured along the acoustic axis through water, normalized to 120 kPa.

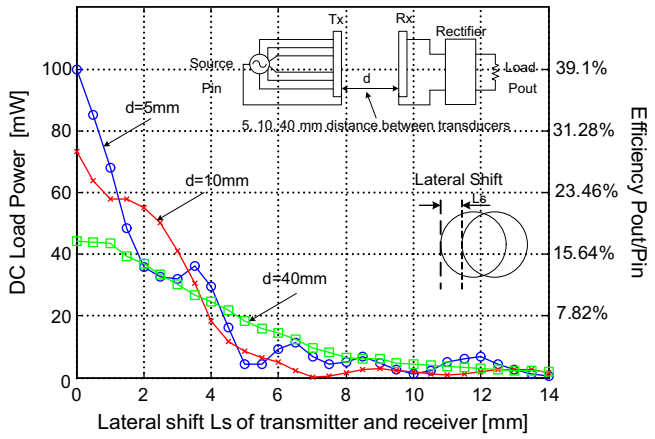

Fig. 16. Measurement results of the harvested electrical power showing dependency on lateral shift *Ls* and axial distance *d* (through pig muscle tissue).

4. Discussion

This work shows the effectiveness of a UTET based on a Gaussian shaded transmitter. Instead of using multiple discrete concentric PZT elements, it is shown that constructing a UTET using a commercially available disc shape PZT element in which both opposing faces are initially fully coated by electrodes and then partitioning one surface electrode into six concentric electrodes is feasible. This is a most practical approach for the transmitter fabrication, rather than using complex shading of the piezoelectric polarization as suggested in [16,17]. Nevertheless, this newly proposed approach implies usage of a power amplifier array. However since the power level is about 100 mW, the whole power amplifier array can be integrated along with the controller as a single ASIC (such as the SCMOS3EE 0.5 μm process, mixed signal CMOS technology used for RFID tags, sensor controllers, display drivers etc., estimated die area of less than 25 mm^2, MHS Electronics, France) excluding the discrete inductors (DO1608C-104, Coilcraft Cary Illinois USA). Using a single ring as the only transmitting element, results in a pressure field with multiple side lobes (Fig. 12), resembling a regular uniformly excited disc, as illustrated in Fig. 13. Nevertheless, by using multiple concentric elements and a Gaussian radial distribution of the excitation voltage, the pressure variations along the acoustic axis through the distance 0–50 mm is less than ±2 dB (Fig 15). In the experiments the excitation voltages had to be calibrated in the range of +/10% to compensate for the inaccuracies of the electrode's sizes of the concentric elements. All simulations and measurements were performed using continuous wave (CW) ultrasound rather than pulsed ultrasound, since pulsed ultrasound is characterized by a higher peak to average pressure ratio than continuous ultrasound for the same level of average pressure. Therefore CW helps to keep the pressure levels in the medium below the safe level dictated by the standards [13] as a Mechanical Index MI and Thermal Index TI (peak pressure measured was 120 kPa giving MI ~0.14 which is lower than the FDA limit of 1.9 (abdominal)). From the perspective of power transfer, while meeting the safety requirements it is better not to generate an intense main pressure lobe which is mandatory for imaging purposes or focused ultrasound applications, instead it is better to spread the power flow over the cross sectional area as much as possible and by doing this it is possible to keep the intensity under the safe limit of 94 mW/cm^2 [12,13]. Although Gaussian beam diverges after the Rayleigh distance compared to a Bessel non-diffracting beam [9,19], the measured pressure which decreased along the acoustic axis, as illustrated in Fig. 15, shows that the axial pressure distribution is almost uniform (to within ±1.9 dB). To measure the power transfer it was decided to use pig muscle tissue (abdominal) since it has much higher attenuation (1–1.8 dB/cm at 1 MHz) than human skin and soft tissue (~0.65 dB/cm at 1 MHz), which helps to estimate the performance envelope. For simple coupling of the transducers to the tissue, the tissue was immersed in the test tank using water as a coupling medium and placed between the transmitter and receiver. The choice of 650 kHz vibration frequency reflects the practical tradeoff between transducer dimensions and power loss within the medium. At 650 kHz, the transmitter construction is quite flat (<5 mm) and lightweight (~10 g) so it can be implemented as a disposable patch adhered to the skin. Nevertheless, due to skin movement, nonoptimal orientation between the transducers can occur. Fig. 16 shows the measured output power (left vertical axis) and power transfer efficiency (right vertical axis) as a function of tissue thickness (d = 5 mm, 10 mm, and 40 mm) and lateral shift ($0 < Ls < 14$ mm recorded every 0.5 mm). Results of the measurements show that the intensity of the pressure field spreads as the distance from the transmitter increases (blue line for the shortest distance of 5 mm, to the green line at 40 mm[1]). The fact that the intensity shape becomes wider as the distance increases from 5 mm to 40 mm causes the lines at different distance d to intersect. In addition, power transfer efficiency rapidly decreases when the lateral shift Ls between the transducers increases to 5 mm (transducer aperture is 7.5 mm). At large distances (40 mm) the power transfer is less sensitive to lateral shift since the pressure field has already spread out as seen in Fig. 14, but at the cost of reduced load power.

Finally, the transducers were chosen to have a radiating surface area of 1.76 cm^2, therefore power transfer of 150 mW can be achieved without exceeding the recommended limit of 94 mW/cm^2 [13] for steady state exposure to ultrasound (abdominal).

5. Conclusions

This paper describes the implementation of a UTET using a stepwise approximation of a Gaussian excitation of the transmitter, to transfer 100 mW to implanted loads. An ordinary single disc PZT element can be used as the base for the transmitter's array. The results of measurements show that even a rough approximation of a Gaussian excitation by six concentric elements is sufficient for generating a pressure field, which results in predictable power transfer. Measured power transfer efficiency was 39.1%, 100 mW at 5 mm distance, reducing to 17.6% and 45 mW at 40 mm. The proposed UTET's transmitter is light (<10 g) and thin (<5 mm) therefore can be produced as a disposable patch to be adhered directly on the skin. The measured results indicate the advantage of a UTET based on a Gaussian shaded transmitter, compared to a uniform excitation of a flat circular piston for a maximal distance of 50 mm.

Acknowledgement

This research was partially supported by the Israel Ministry of Science and Technology under Grant No. 3-4772.

References

[1] G. Vandevoorde, R. Puers, Wireless energy transfer for standalone systems: a comparison between low and high power applicability, Sensors and Actuators 92 (1–3) (2001) 305–311.
[2] Uei-Ming Jow, Maysam Ghovanloo, Modeling and optimization of printed spiral coils in air, saline, and muscle tissue environments, IEEE Transaction on Biomedical Circuits and Systems 3 (5) (2009) 339–347.
[3] A Chua-Chin Wang, Tzung-Je Lee, Yu-Tzu Hsiao, U Fat Chio, Chi-Chun Huang, Jia-Jin J. Chin, Ya-Hsin Hsueh, A multiparameter implantable microstimulator

[1] For interpretation of color in Figs. 2, 3, 5, 7–10, 12–16, the reader is referred to the web version of this article.

SOC, IEEE Transactions on Very Large Scale Integration (VLSI) Systems 13 (12) (2005) 1399–1402.
[4] Chi-Chun Huang, Shou-Fu Yen, Chua-Chin Wang, A Li-ion battery charging design for biomedical implants, APCCAS IEEE Asia Pacific Conference on Circuits and Systems 30 (3) (2008) 400–403.
[5] G.V.B. Cochran, M.P. Kadaba, V.R. Palmieri, External ultrasound can generate microampere direct currents in vivo from implanted piezoelectric materials, Journal of Orthopaedic Research 6 (1988) 145–147.
[6] S. Ozeri, D. Shmilovitz, Ultrasonic transcutaneous energy transfer for powering implanted devices, Ultrasonics 50 (6) (2010) 556–566.
[7] D.T. Blackstock, Physical Acoustics, John Wiley Publications, 2000. pp. 440–457.
[8] J. Zemanek, Beam behavior within the near field of a vibrating piston, Journal of the Acoustical Society of America 49 (1971) 181–191.
[9] J.A. Campbell, S. Soloway, Generation of a nondiffracting beam with frequency independent beamwidth, Journal of the Acoustical Society of America 88 (5) (1990) 2467–2477.
[10] J. Durnin, Miceli Jr., Diffraction-free beams, Physical Review Letters 58 (15,13) (1987) 1499–1501.
[11] H. Masuyama, T. Yokoyama, K. Nagai, K. Mizutani, Generation of Bessel beam from equiamplitude-driven annular transducer array consisting of a few elements, Japanese Journal of Applied Physics 38 (1999) 3080–3084.
[12] S. Felkel, Ultrasound safety: mechanical and thermal indices: a primer, Journal of Diagnostic Medical Sonography 15 (1999) 77–80.
[13] US Department of Health and Human Services, Food and Drug Administration, Center for Devices and Radiological Health, Information for Manufacturers Seeking Marketing Clearance of Diagnostic Ultrasound Systems and Transducers, 9 September 2008.
[14] D. Huang, M. Breazeale, An ultrasonic gaussian transducer and its diffraction field, IEEE Transactions on Ultrasonics, Ferroelectrics and Frequency Control 53 (5) (2006) 1018–1027.
[15] J.F. Kelly, R.J. McGough, An annular superposition integral for axisymmetric radiators, Journal of the Acoustical Society of America 121 (2) (2007) 759–765.
[16] H. Calas et al., Non-uniformly polarized piezoelectric modal transducer: fabrication method and experimental results, Smart Materials and Structures 15 (2006) 904–908.
[17] D.K. Hsu et al., Non-uniformly poled gaussian and Bessel function transducers, Ultrasonics Symposium (1989) 789–792.
[18] K.A. Snook, C.-H. Hu, T.R. Shrout, K. Shung, High frequency ultrasound annular array imaging. Part I: array design and fabrication, IEEE Transactions on Ultrasonics, Ferroelectrics and Frequency Control 53 (2) (2006) 300–308.
[19] Jian-Yu Lu, James F. Greenleaf, Ultrasonic nondiffracting transducer for medical imaging, IEEE Transactions on Ultrasonics, Ferroelectrics and Frequency Control 37 (5) (1990) 438–447.
[20] T. Inoue, M. Ohta, S. Takahashi, Design of ultrasonic transducers with multiple acoustic matching layers for medical application, IEEE Transactions on Ultrasonics, Ferroelectrics and Frequency Control UFFC-34 (1) (1987) 8–16.
[21] S. Ben-Yaakov, N. Krihely, Resonant rectifier for piezoelectric sources, IEEE Applied Power Electronics Conference, APEC (2005) 249–253.
[22] K.C. Cheng, H.L.W. Chan, Characterization of piezoelectric ring used for wire bonding transducer application, in: Electron Device Meeting, Proceedings, Hong Kong, 2001, pp. 64–67.
[23] P.A. Lewin, H. Busk, In-vivo ultrasonic measurements of tissue properties, Ultrasonics Symposium (1982) 709–712.
[24] R.A. Eno, Pyrolytic Carbon Transmyocardial Implant, United States Patent 6113823, 09/05/2000.
[25] Pyrolytic carbon for biomedical applications, <http://www.azom.com/details.asp>, 2008 (accessed 6.08).
[26] J.R. Davis, Handbook of Materials for Medical Devices, ASM International (2003).
[27] P.J. Kielczynski, W. Pajewski, M. Szalewski, Ring piezoelectric transducers radiating ultrasonic energy into the air, IEEE Transactions on Ultrasonics, Ferroelectrics and Frequency Control 37 (1) (1990) 38–43.
[28] <http://www.kayelaby.npl.co.uk/general_physics/2_4/2_4_6.html>, 2009 (accessed 11.09).
[29] Francis A Duck, Andrew C Baker, Hazel C Starritt, Ultrasound in Medicine, Institute of Physics Publishing, 1998, pp. 57–88.
[30] P.J. Stevenson, D.A. Hall, Characteristic P-E and S-E relationships of hard PZT ceramics under high drive conditions, in: Proceedings of the Tenth IEEE International Symposium on Applications of Ferroelectrics. ISAF, vol. 1, August 1996, pp. 313–316.
[31] R.W. Erickson, D. Maksimovic, Fundamentals of Power Electronics, second ed., Kluwer Academic Publishing, 2001, pp. 709–721.